CrossMark

A Comprehensive Study of One-Step Selenization Process for Cu(In$_{1−x}$Ga$_x$)Se$_2$ Thin Film Solar Cells

Shih-Chen Chen[1*] , Sheng-Wen Wang[2], Shou-Yi Kuo[3,4], Jenh-Yih Juang[1], Po-Tsung Lee[2], Chih Wei Luo[1], Kaung-Hsiung Wu[1*] and Hao-Chung Kuo[2*]

Abstract

In this work, aiming at developing a rapid and environmental-friendly process for fabricating CuIn$_{1−x}$Ga$_x$Se$_2$ (CIGS) solar cells, we demonstrated the one-step selenization process by using selenium vapor as the atmospheric gas instead of the commonly used H$_2$Se gas. The photoluminescence (PL) characteristics indicate that there exists an optimal location with superior crystalline quality in the CIGS thin films obtained by one-step selenization. The energy dispersive spectroscopy (EDS) reveals that the Ga lateral distribution in the one-step selenized CIGS thin film is intimately correlated to the blue-shifted PL spectra. The surface morphologies examined by scanning electron microscope (SEM) further suggested that voids and binary phase commonly existing in CIGS films could be successfully eliminated by the present one-step selenization process. The agglomeration phenomenon attributable to the formation of MoSe$_2$ layer was also observed. Due to the significant microstructural improvement, the current–voltage (*J-V*) characteristics and external quantum efficiency (EQE) of the devices made of the present CIGS films have exhibited the remarkable carrier transportation characteristics and photon utilization at the optimal location, resulting in a high conversion efficiency of 11.28%. Correlations between the defect states and device performance of the one-step selenized CIGS thin film were convincingly delineated by femtosecond pump-probe spectroscopy.

Keywords: Selenization, CIGS, Solar cell, MoSe$_2$, Pump-probe spectroscopy

Background

CuIn$_{1−x}$Ga$_x$Se$_2$ (CIGS) has emerged as one of the most promising materials for low cost and high-efficiency thin-film solar cells. CIGS possesses superior optical properties such as high absorption coefficient ($\alpha \sim 10^5$ cm^{-1}), long-term stability, and high radiation tolerance, due to that it belongs to the family of direct band gap chalcopyrite semiconductor compounds. Moreover, its band gap can be engineered by the partial substitution of indium by gallium, which further renders the flexibility of manipulating the optical absorption [1]. Nowadays, various methods for preparing CIGS absorber layers have been implemented, including vacuum processes (co-evaporation [2], sputtering [3], and pulsed laser deposition [4]) and nonvacuum processes (ink-printing [5] and electrochemical deposition [6]). However, the high quality CIGS thin films for laboratory-scale or module-level solar cells are usually prepared by co-evaporation or sputtering processes. In general, co-evaporation and sputtering processes for growing CIGS thin films both include the metallic precursor deposition of Cu–In–Ga alloy and the subsequent two-step selenization process, which consists of an initial low temperature selenization in H$_2$Se atmosphere followed by a high temperature annealing in inert gas. By precisely controlling the parameters of selenization, it has been demonstrated that homogeneous CIGS films with tunable in-depth Ga distribution can be obtained, such that the open-circuit voltage (V_{oc}) of the devices can be increased due to the formation of the Ga-rich surface layer [7, 8].

* Correspondence: cscbobo@gmail.com; khwu@cc.nctu.edu.tw; hckuo@faculty.nctu.edu.tw
[1]Department of Electrophysics, National Chiao-Tung University, Hsinchu, Taiwan
[2]Department of Photonics and Institute of Electro-Optical Engineering, National Chiao-Tung University, Hsinchu, Taiwan
Full list of author information is available at the end of the article

Chen *et al. Nanoscale Research Letters* (2017) 12:208

Page 2 of 6

However, owing to the increasing environmental concerns on the green energy issues, the researchers are still seeking for yet more environmental friendly and simpler selenization processes for preparing CIGS thin films. To this respect, here, we report a one-step selenization process by using selenium (Se) vapor as the atmospheric gas instead of the commonly used H_2Se gas. The photoluminescence (PL) intensity mapping image and spectra of the one-step selenized CIGS thin film indicate that there exists an optimal location exhibiting completed stoichiometric reaction with the introduced Se vapor flux. The lateral distribution of Ga and the inhomogeneous surface morphology of the one-step selenized CIGS film were examined by energy dispersive spectroscopy (EDS) and scanning electron microscope (SEM) to delineate the prominent role played by Ga-doping. The current–voltage (*J-V*) characteristics and external quantum efficiency (EQE) of the devices made from different locations of the one-step selenized CIGS thin film were measured to reveal its correlations with film stoichiometry. Finally, the ultrafast carrier dynamics at different locations of the CIGS film were probed with femtosecond (fs) optical-pump optical-probe spectroscopy to elaborate the key mechanism governing the efficiency of CIGS solar cells.

Methods

Farbrication of CIGS Thin Film Solar Cells

The metallic precursors, $Cu_{0.75}Ga_{0.25}$ and elemental In targets, were deposited on a Mo-coated soda-lime glass (SLG) substrate (100 mm × 100 mm) by dc-magnetron sputtering. The precursor elements were co-sputtered at room temperature, and the substrate was rotated continuously during deposition. The Cu–In–Ga alloy (thickness ~0.6 μm) was formed at the working pressure of 3×10^{-3} mbar. The Cu/(In + Ga) and Ga/(Ga + In) atomic ratios of the precursor were 0.9 and 0.25, respectively. Subsequently, the Cu–In–Ga metallic precursor was inserted into a quartz furnace for one-step selenization process (see the schematic illustration shown Fig. 1). The reaction under the Se vapor was conducted in a horizontal
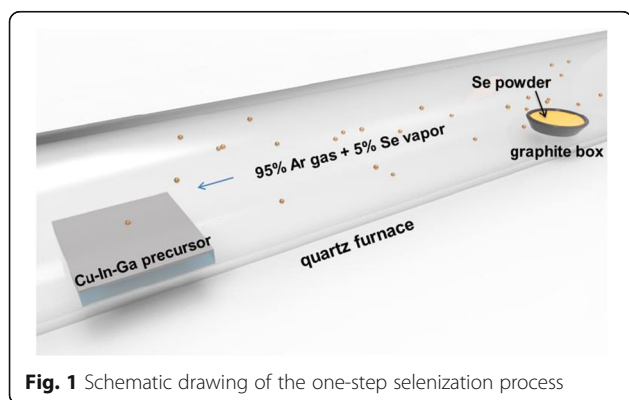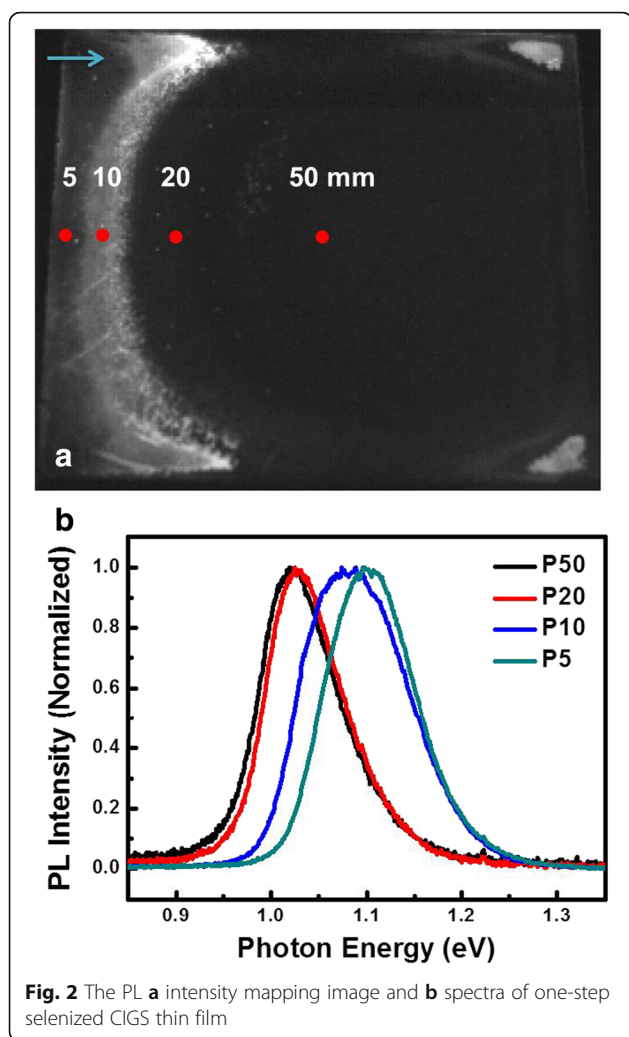
tube reactor at pressure of 450–500 Torr. The Se vapor was diluted in the Ar gas atmosphere with 5% molar concentration during the one-step selenization process. The substrate temperature was raised from room temperature to 550 °C within 25 min. The selenization reaction time was longer than 20 min at 550 °C. For device fabrications, a CdS buffer layer (50–70 nm) was deposited by chemical bath deposition (CBD) for *p-n* junction formation. An insulating ZnO (i-ZnO) winder layer and an Al-doped ZnO (AZO) transparent conductive oxide layer were capped on the *p-n* junction. Finally, the silver grid pattern was coated as the top layer by the printing process. The different CIGS solar cells were obtained from the 100×100 mm^2 substrate using a mechanical scribe.

Characterizations

A 635-nm diode laser was employed to excite the sample for PL measurements. The PL intensity mapping image and spectra were acquired by infrared (IR) camera and photomultiplier tube (PMT), respectively. The surface morphologies of the CIGS thin film were examined by scanning electron microscopy (SEM, JSE-7001, JEOL, Tokyo, Japan). Composition information of the samples were analyzed by using energy dispersive spectrometer (EDS, INCA analysis system, Oxford Instruments, Oxford shire, UK) at an accelerating voltage of 15 kV with the sampling depth of about 1 μm. *J-V* characteristics of the devices were measured following the procedures described in the international standard CEI IEC 60904-1. The cells were characterized under a simulated Air Mass 1.5, Global (AM1.5G) illumination with a power of 1000 W/m^2. The external quantum efficiency (EQE) of devices was measured by a 300-W xenon lamp (Newport 66984) light source with a monochromator (Newprot 74112). The EQE data were acquired using a lock-in amplifier (Stanford Research System, SR830) with an optical chopper unit (SR540) operated at 260 Hz chopping frequency and a 1Ω resistor in shunt connection to convert the photocurrent into voltage.

Results and Discussion

Figure 2a shows the PL intensity mapping image over an area of 100×100 mm^2 CIGS thin film prepared by the one-step selenization process measured at room temperature with an excitation power of 3 mW. It can be seen that the one-step selenization process has resulted in a rather non-uniform distribution of PL intensity. Figure 2b displays the room-temperature PL spectrum of each point taken at different distances (5, 10, 20, 50 mm) from the left edge (The incoming direction of Se vapor flux is denoted by the arrow.) of the sample (indicated by the red dots shown in Fig. 2a) and are denoted as P5, P10, P20, and P50, respectively. The energy of the PL emission peak was within the range of

Fig. 1 Schematic drawing of the one-step selenization process

Chen *et al. Nanoscale Research Letters* (2017) 12:208

Page 3 of 6

Fig. 2 The PL **a** intensity mapping image and **b** spectra of one-step selenized CIGS thin film

about 1.03 ~ 1.12 eV, agreeing well with the band gap of CIGS (~1.1 eV) [9]. It is noted that the noticeable blue shift of PL emission peak energy from P50 to P5 implicates the variation of compositions at these locations. The elemental compositions at different film locations determined by EDS analyses are listed in Table 1. From the results, it is evident that at P20 and P50 the film is essentially gallium-free (Ga = 0), presumably due to the off-stoichiometry reaction resulted from unavailable in-depth Ga distribution. Nevertheless, the Ga/(Ga + In) ratio is substantially increased to 0.16 and 0.18 for P10

and P5, respectively. Such a stoichiometry change may account for the blue-shifted PL spectra displayed in Fig. 2b. In contrast, the amount of In exhibits a changing trend opposite to that of Ga. This phenomenon of inhomogeneous selenization can be attributed to the cracked flux of Se vapor during the reaction [10].

Figure 3 shows the top-view and side-view SEM images taken at different locations of the CIGS thin films prepared by the one-step selenization process. Figure 3a–d shows the top-view SEM images for P50, P20, P10, and P5, respectively. From the surface morphology, it is apparent that at P50 (Fig. 2a) and P20 (Fig. 2b) the grain structure consists of irregular-shape grains and some distributed needle-like grains, suggesting that in these regions the film is mainly a mixture of off-stoichiometry binary phases (i.e., InSe and In_2Se) [11, 12]. The grains of irregular morphology at P50 and P20 may also relate to the residual Cu_2Se binary phase [13]. In any case, the appearance of those binary phases is also consistent with the gallium-free phenomenon observed at P50 and P20. Moreover, the voids between CIGS thin film and Mo back contact were observed at P50 and P20 (see Fig. 3e, f), which can further lead to deteriorated carrier transportation, and hence the performance of the devices. In contrast, the chunk-shape grain morphology observed at P10 and P5 (see Fig. 3c, d) suggests the Cu-poor characteristic in these regions [7], which is also consistent with the lower Cu/(In + Ga) ratios, 0.87 and 0.85, for P10 and P5, respectively. The cross-sectional view SEM image of P10 (Fig. 3g) exhibits a feature of grain agglomeration, which can be attributed to the formation of the $MoSe_2$ layer between CIGS thin film and Mo back contact [14, 15]. It is believed that, by introducing Se vapor flux with the present scheme, complete selenization was achieved at an optimal location near P10, which, in turn, results in the superior crystalline quality as well as the higher PL intensity observed in Fig. 2a.

Figure 4a exhibits the current–voltage (*J-V*) characteristics for the devices made from areas at different locations of the one-step selenized CIGS thin film. The corresponding device performance parameters are listed in Table 2. The larger V_{oc}'s obtained for devices made of films at P10 and P5 can be related to the enlarged bandgap resulted from increasing Ga content [16]. In particular, it is noted that the fill factor (FF) is significantly enhanced at location of P10, presumably owing to the agglomeration of grain structures and the formation of the $MoSe_2$ layer, which may have greatly modified the carrier transportation. Consequently, the highest conversion efficiency of 11.28% has been achieved at location of P10. (The conversion efficiencies of two-step selenized CIGS thin film solar cells with the same Cu–In–Ga precursor were averagely distributed at 11%.) The external
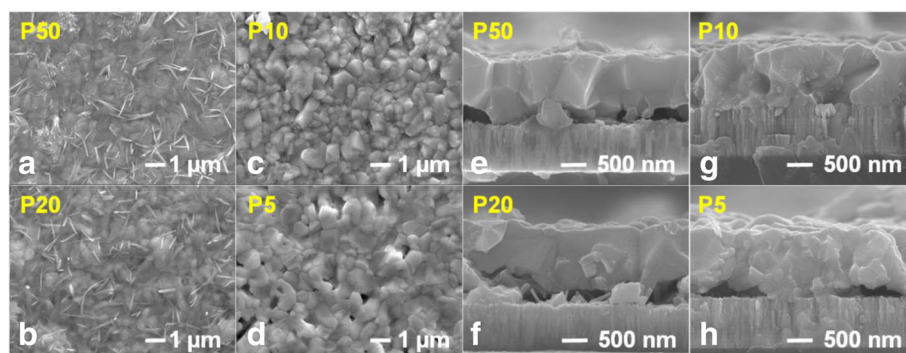
Table 1 Compositions for different locations at one-step selenized CIGS thin film

Location (mm)	Cu (at.%)	Se (at.%)	Ga (at.%)	In (at.%)	$\frac{Cu}{(Ga+In)}$	$\frac{Ga}{(Ga+In)}$
5	21.39	53.50	4.54	20.57	0.85	0.18
10	21.31	54.17	3.87	20.65	0.87	0.16
20	24.03	49.56	0	26.41	0.91	0
50	25.46	48.53	0	26.01	0.98	0

Chen *et al. Nanoscale Research Letters* (2017) 12:208

Page 4 of 6

Fig. 3 The *top-view* (**a**–**d**) and *side-view* (**e**–**h**) SEM images for different locations of one-step selenized CIGS

quantum efficiency (EQE) measurements were also conducted at the four positions as shown in Fig. 4b. The EQE loss observed in the wavelength region of 400–500 nm is due to the absorption of CdS buffer layer. At long wavelength region, the cut-off wavelengths of P5 and P10 were blue-shifted that are consistent with the enlarged band gap of CIGS thin films (Fig. 2b). It is also evident that the modification of grain

structures and stoichiometric composition at P10 are beneficial to a broadband enhancement of photon utilization, leading to the higher short-circuit current density exceeding 30 mA/cm^2.

In order to investigate the defects existing in the one-step selenized CIGS thin film, the femtosecond pump-probe spectroscopy measurement was carried out, which is a powerful technique to delineate non-equilibrium carrier dynamics in the present CIGS films [17, 18]. Upon the illumination of the pumping pulses from the femtosecond laser, a large amount of carriers are expected to be excited in the CIGS thin film. The subsequent carrier relaxation processes are then to be probed by a sequence of probing pulses, which are simultaneously reflected on the reflectivity transient ($\triangle R/R$). The semi-log plots of the $\Delta R/R$ for different locations obtained at the one-step selenized CIGS are plotted in Fig. 5a. The curves are fitted with a bi-exponential decay function, $[A_1\exp(-t/\tau_1) + A_2\exp(-t/\tau_2)]$, with τ_1 and τ_2 being related to hot carrier relaxation and defect-related recombination, respectively. It is apparent from the results that the longest defect-related carrier lifetime (τ_2) is obtained at location of P10, suggesting the minimum density of defect states in this region [17], which is well consistent with the much superior crystalline quality in this region described above. The magnitudes of the defect-related carrier lifetime (τ_2) are further compared with conversion efficiency in Fig. 5b. The nearly one-to-one correspondence has convincingly confirmed the intimate correlation between the density of defect states and the conversion efficiency of the devices.
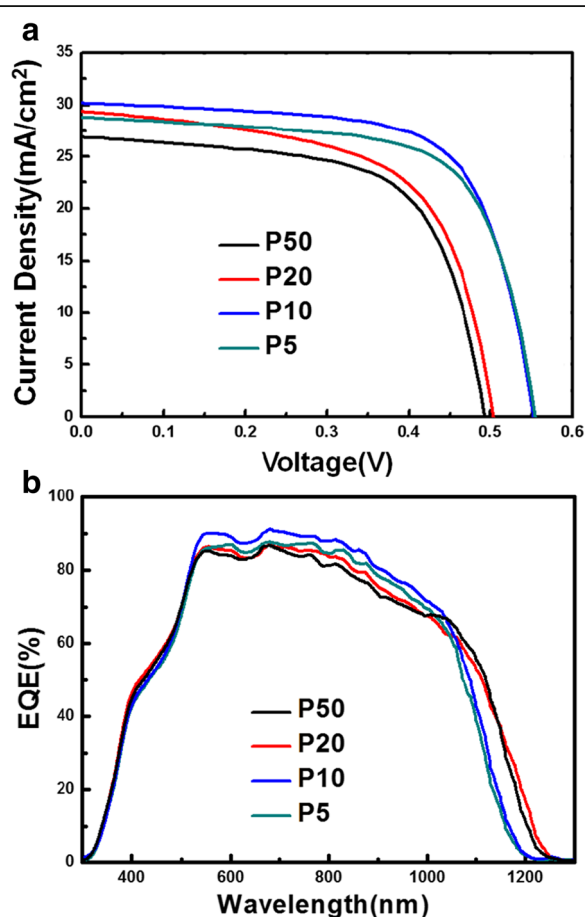

Fig. 4 a *J-V* and **b** EQE measurements for different locations of one-step selenized CIGS

Table 2 *J-V* characteristics for different locations of one-step selenized CIGS

Location	V_{oc}(mV)	J_{sc}(mA/cm^2)	FF(%)	Efficiency(%)
P5	556	28.76	67	10.75
P10	553	30.18	68	11.28
P20	505	29.39	60	8.95
P50	494	26.91	64	8.48

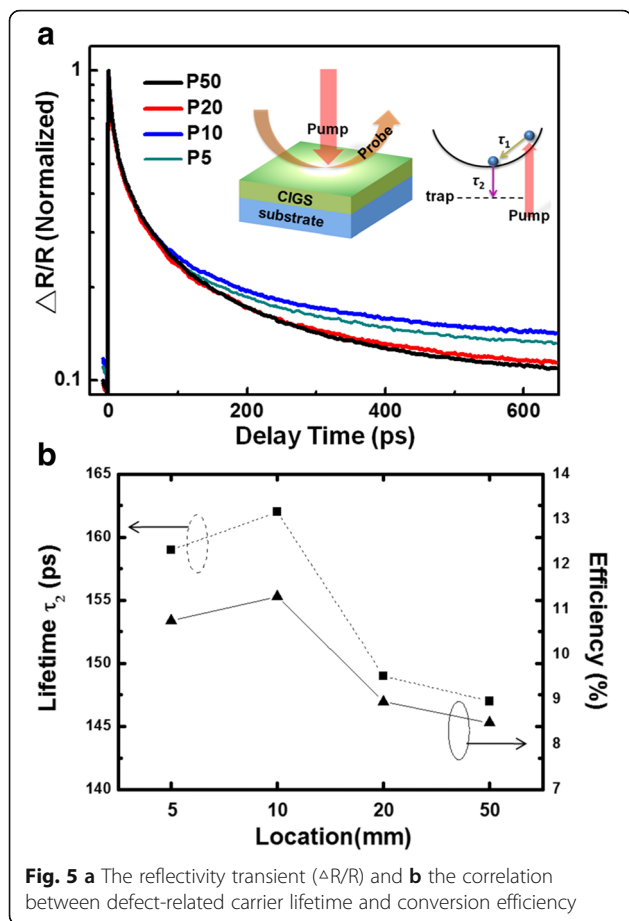Chen *et al. Nanoscale Research Letters* (2017) 12:208

Page 5 of 6

Fig. 5 a The reflectivity transient (△R/R) and **b** the correlation between defect-related carrier lifetime and conversion efficiency

Conclusions

In summary, we have successfully demonstrated that the one-step selenization process using selenium vapor instead of H_2Se can meet the demand of high efficiency and environmental friendly method for preparing high-quality CIGS thin films. The photoluminescence intensity mapping image obtained from the one-step selenized CIGS thin film suggested that there exists an optimal location (P10) for obtaining CIGS film with superior crystalline quality. The blue-shifted photoluminescence spectra obtained from the regions at P5 and P10 are consistent with the lateral distribution of Ga element as revealed by energy dispersive spectroscopy (EDS). According to the surface morphologies examined by scanning electron microscope, it is evident that the binary phase and voids of one-step selenized CIGS film can be eliminated at the P10, with agglomeration of grain and the formation of a $MoSe_2$ layer. Consequently, the current-voltage characteristics and external quantum efficiency of the devices made of film regions near P10 exhibited characteristics of highly efficient carrier transportation and remarkable photon utilization, which are intimately related to the improvements of grain structures and stoichiometric composition. Finally, the femtosecond pump-probe spectroscopy studies unambiguously revealed the close correlations between the defect-related carrier lifetime, density of defect states, and the conversion efficiency of the devices. The present results indicate that the one-step selenization process might serve as a viable avenue for developing the high-efficiency CIGS solar cells.

Abbreviations
CBD: Chemical bath deposition; CIGS: $CuIn_{1-x}Ga_xSe_2$; EDS: Energy dispersive spectrum; EQE: External quantum efficiency; FF: Fill factor; IR: Infrared; PL: Photoluminescence; PMT: Photomultiplier tube; SEM: Scanning electron microscope; SLG: Soda-lime glass

Authors' Contributions
CSC, WSW, and KSY carried out the thin film growth, scanning electron microscopy, pump-probe analysis, and device fabrications and drafted the manuscript. JJY and LPT carried out the PL analysis. LCW participated in the design of the study. WKH and KHC conceived the study and organized the final version of the paper. All authors read and approved the final manuscript.

Competing Interests
The authors declare that they have no competing interests.

Publisher's Note
Springer Nature remains neutral with regard to jurisdictional claims in published maps and institutional affiliations.

Author details
[1]Department of Electrophysics, National Chiao-Tung University, Hsinchu, Taiwan. [2]Department of Photonics and Institute of Electro-Optical Engineering, National Chiao-Tung University, Hsinchu, Taiwan. [3]Department of Electronic Engineering, Chang Gung University, Taoyuan, Taiwan. [4]Department of Nuclear Medicine, Chang Gung Memorial Hospital, Taoyuan, Taiwan.

References
1. Mezher M, Garris R, Mansfield LM, Horsley K, Weinhardt L, Duncan DA, Blum M, Rosenberg SG, Bär M, Ramanathan K, Heske C (2016) Electronic structure of the Zn(O, S)/Cu(In, Ga)Se2 thin film solar cell interface. Prog Photovolt Res Appl 24:1142–1148
2. Jackson P, Hariskos D, Lotter E, Paetel S, Wuerz R, Menner R, Wischmann W, Powalla M (2011) New world record efficiency for Cu(In, Ga)Se2 thin-film solar cells beyond 20%. Prog Photovolt Res Appl 19:894–897
3. Chang JC, Chuang CC, Guo JW, Hsu SC, Hsu HR, Wu CS, Hsieh TP (2011) An investigation of CuInGaSe2 thin film solar cells by using CuInGa precursor. Nanosci Nanotechnol Lett 3:200–203
4. Chen SC, Hsieh DH, Jiang H, Liao YK, Lai FI, Chen CH, Luo CW, Juang JY, Chueh YL, Wu KH, Kuo HC (2014) Growth and characterization of Cu(In, Ga)Se2 thin films by nanosecond and femtosecond pulsed laser deposition. Nanoscale Res Lett 9:280

Chen *et al. Nanoscale Research Letters* (2017) 12:208

Page 6 of 6

5. Chen SC, Chen YJ, Chen WT, Yen YT, Kao TS, Chuang TY, Liao YK, Wu KH, Yabushita A, Hsieh TP, Charlton MDB, Tsai DP, Kuo HC, Chueh YL (2014) Toward omnidirectional light absorption by plasmonic effect for high-efficiency flexible nonvacuum Cu(In,Ga)Se$_2$ thin film solar cells. ACS Nano 8(9):9341–9348

6. Calixto ME, Dobson KD, McCandless BE, Birkmire RW (2006) Controlling growth chemistry and morphology of single-bath electrodeposited Cu(In, Ga)Se2 thin films for photovoltaic application. J Electrochem Soc 153:G521–G528

7. Marudachalam M, Hichri H, Klenk R, Birkmire RW, Shafarman WN, Schultz JM (1995) Preparation of homogeneous Cu(InGa)Se$_2$ films by selenization of metal precursors in H$_2$Se atmosphere. Appl Phys Lett 67:3978

8. Liang H, Avachat U, Liu W, van Duren J, Le M (2012) CIGS formation by high temperature selenization of metal precursors in H$_2$Se atmosphere. Solid State Electron 76:95–100

9. Shimakawa S, Kitani K, Hayashi S, Satoh T, Hashimoto Y, Takahashi Y, Negami T (2006) Characterization of Cu(In, Ga)Se2 thin films by time-resolved photoluminescence. Phys Status Solidi A 203:2630–2633

10. Lia G, Liu W, Liu Y, Lin S, Zhang Y, Zhou Z, He Q, Sun Y (2015) The influence of cracked selenium flux on CIGS thin film growth and device performance prepared by two-step selenization processes. Sol Energy Mater Sol Cells 139:108–114

11. Kim K, Hanket GM, Huynh T, Shafarman WN (2012) Three-step H2Se/Ar/H2S reaction of Cu-In-Ga precursors for controlled composition and adhesion of Cu(In, Ga)(Se, S)2 thin films. J Appl Phys 111:083710

12. Lin YC, Lin ZQ, Shen CH, Wang LQ, Ha CT, Peng C (2012) Cu(In,Ga)Se$_2$ films prepared by sputtering with a chalcopyrite Cu(In,Ga)Se$_2$ quaternary alloy and In targets. Mater Electron 23:493–500

13. Hsieh TP, Chuang CC, Wu CS, Chang JC, Guo JW, Chen WC (2011) Effects of residual copper selenide on CuInGaSe$_2$ solar cells. Solid-State Electron 56:175–178

14. Hsiao KJ, Liu JD, Hsieh HH, Jiang TS (2013) Electrical impact of MoSe$_2$ on CIGS thin-film solar cells. Phys Chem Chem Phys 15:18174–18178

15. Jeon CW, Cheon T, Kim H, Kwon MS, Kim SH (2015) Controlled formation of MoSe$_2$ by MoNx thin film as a diffusion barrier against Se during selenization annealing for CIGS solar cell. J Alloys Compd 644:317–323

16. Topič M, Smole F, Furlan J (1996) Band-gap engineering in CdS/Cu(In, Ga)Se2 solar cells. J Appl Phys 79:8537–8540

17. Chen SC, Liao YK, Chen HJ, Chen CH, Lai CH, Chueh YL, Kuo HC, Wu K H, Juang JY, Cheng SJ, Hsieh TP, Kobayashi T (2012) Ultrafast carrier dynamics in Cu(In,Ga)Se$_2$ thin films probed by femtosecond pump-probe spectroscopy. Opt. Express 20: 12675–12681

18. Chen SC, Wu KH, Li JX, Yabushita A, Tang SH, Luo CW, Juang JY, Kuo HC, Chueh YL (2015) In-situ probing plasmonic energy transfer in Cu(In, Ga)Se$_2$ solar cells by ultrabroadband femtosecond pump-probe spectroscopy. Sci Rep 5:18354